Article

Journal of
Nanoscience and Nanotechnology
Vol. 15, 4530–4533, 2015
www.aspbs.com/jnn

Effects of Processing Temperatures of Nickel Plating on Capacitance Density of Alumina Film Capacitor

Myung-Sun Jeong[1,2], Byeong-Kwon Ju[2], and Jeon-Kook Lee[1,*]

[1] Interface Control Research Center, Korea Institute of Science and Technology, 14 Hwarang-ro Seongbook, Seoul 136-791, Republic of Korea
[2] Display and Nanosystem Laboratory, College of Engineering, Korea University, Anam-dong, Seongbuk-gu, Seoul 136-713, Republic of Korea

We observed the effects of nickel plating temperatures for controlling the surface morphologies of the deposited nickel layers on the alumina nano-pores. The alumina nano-channels were filled with nickel at various processing temperatures of 60∼90 °C. The electrical properties of the alumina film capacitors were changed with processing temperatures. The electroless nickel plating (ENP) at 60 °C improved the nickel penetration into the alumina nano-channels due to the reduced reaction rate. Nickel layers are uniformly formed on the high aspect ratio alumina pores. Due to the uniform nickel electrode, the capacitance density of the alumina film capacitors is improved by the low leakage current, dissipation factor and equivalent series resistance. Alumina film capacitors made by ENP at 60 °C had a high capacitance density of 160 nF/cm^2.

Keywords: Alumina Film Capacitor, Electroless Plating, Alumina Nano-Channel, Nickel Electrode, Processing Temperature.

1. INTRODUCTION

Developments of electrical devices such as automotive electronics and cellular phones require the capacitors with a high electrical energy density. Capacitors using electrolytes are widely used because of their low cost and small size.[1–3]

Nevertheless, they are limited by a narrow range of operating temperature as well as a polarity by liquid electrode. The all solid capacitors that have metal electrodes instead of liquid electrolytes electrode in the nanopore alumina capacitors have the advantages of high voltage, a wide range of operating temperature, and excellent frequency properties.[4]

The all solid capacitor is composed of a nickel electrode formed by electroplating (EP)[5,6] and atomic layer deposition (ALD).[7] In contrast to the deposition methods like EP and ALD, electroless nickel plating (ENP) is used to deposit the metals onto high aspect ratio nano-structured alumina insulators.

Ting et al. studied a nickel electrode selectively deposited on via hole of 1.5 μm × 1.5 μm nominal size by electroless plating in an aqueous solution of dimethylamineborane and hypophosphite as reducing agents.[8] Wang et al. reported that electroless copper was plated on TaN/SiO_2/Si substrates with holes of a diameter from 0.31 μm to 1.0 μm and a depth of 2.3 μm.[9] Both groups obtained ENP on the patterned substrate with a low aspect ratio.

Jang et al. developed a film capacitor with a high aspect ratio alumina nano-structure with a depth of 40 μm and a diameter of 1 μm using ENP.[3] However, the via hole blockings of ENP particles are the main problems in all solid capacitors.

Processing temperature affects the deposition rate in ENP. Deposition rates of ENP at 90 °C are 25–30 μm/h. The deposition rate of nickel decreases as the processing temperature decreases. Below 65 °C and above 90 °C, ENP processing become unstable.[10,11]

A low ENP processing temperature improves the nickel penetration into the alumina nano-channels due to the reduced reaction rate. Nickel particles on the alumina nano-channels are uniformly distributed.

In this research, we observed the effects of the ENP processing temperatures on the deposition rate and morphologies of the deposited nickel particles on the alumina nano-channels.

*Author to whom correspondence should be addressed.

1533-4880/2015/15/4530/004 doi:10.1166/jnn.2015.9781

2. EXPERIMENTAL DETAILS

We use the alumina film capacitors supported by Samyoung Electronics Co., Korea. The alumina nano-channels are well-aligned. The diameter and depth of the alumina pore channel were 1 μm and 50 μm, respectively. The alumina surface had a high roughness due to hydrated alumina for a high aspect ratio as shown in Figure 1.

Alumina nano-channel substrate of 1×1 cm^2 was partially covered with polyimide tape to make the active area for electrical measurements. The substrates were chemically activated for 5 seconds by a catalyst of 0.1 g/L $PdCl_2$ and 0.1 ml/L HCl aqueous solutions. The activated specimens were immersed in a liquid solution with polyethylene glycol (PEG, 3400 MW, 0.1 mM) to prevent paladium blocking in the entrance of the aluminum tunnels.[3] ENP on the alumina nano-channels was carried out in an acid solution (pH 4.6) of commercial solution of Hanbit EPN (Hanbit Chemical, Korea) based on sodium hypophosphite baths. The alumina nano-channels were filled with nickel at various processing temperatures of 60∼90 °C.

The microstructures were observed by focused ion beam scanning electron microscopy (FIB-SEM, Nova 600 Nanolab, FEI, USA) and field emission scanning electron microscopy (FE-SEM, XL-30 FEG, FEI, USA) at an acceleration voltage of 15 kV. The coating composition was determined by energy dispersive spectrometry (EDS). The capacitance density was measured using an impedance analyzer (Agilent 4294A, USA) at 1 MHz. The current density versus voltage characteristics were measured by a semiconducting parameter analyzer (Keithley-4200, USA). To avoid complete dielectric breakdown, compliance current was used to limit the current flow.

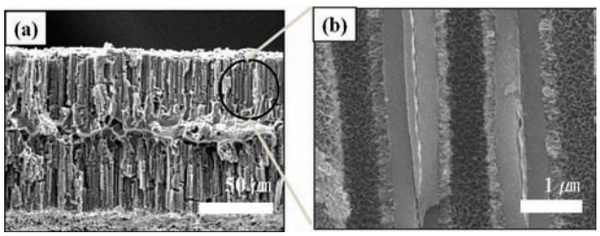

Figure 1. Cross-sectional morphologies of the alumina nano-channels: (a) low magnification and (b) high magnification.

3. RESULTS AND DISCUSSION

The effects of the ENP temperatures on the nickel particles penetration are shown in Figure 2. Figure 2(a) shows the cross-sectional microstructure of the alumina nano-channels without nickel penetration. Nickel particles with 250 nm diameters formed in the upper part of the alumina nano-channels at a fast ENP at 90 °C, as shown in Figure 2(b). However, as shown in Figure 2(c), the nickel

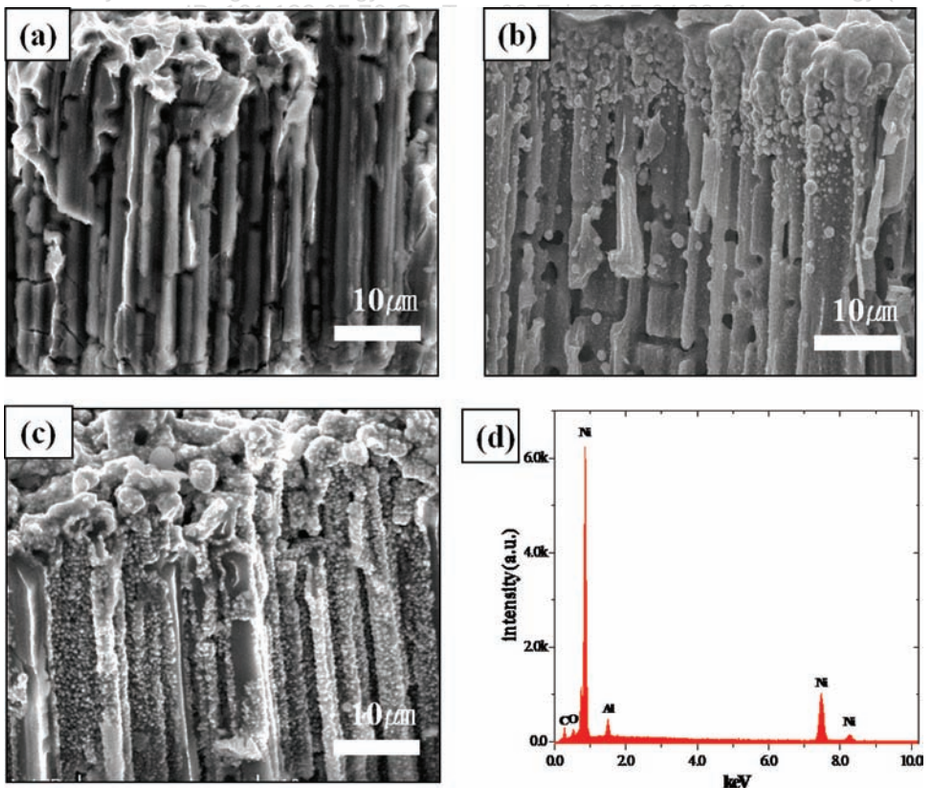

Figure 2. Cross-sectional images of (a) alumina nano-channels without nickel particles; (b) alumina nano-channels with nickel made by ENP at 90 °C, (c) 60 °C and (d) EDS data for alumina and nickel layers.

particles with diameters of 30 nm formed through the alumina nano-channels due to the effect of a low processing temperature of 60 °C.

The overall processes for ENP can be represented by the following reaction.

$$H_2PO_2^- + H_2O = HPO_3^{2-} + H^+ + 2H_{ad} \tag{1}$$

$$2H_{ad} + Ni^+ = Ni + 2H^+ \tag{2}$$

$$H_2PO_2 + H_{ad} = H_2O + OH^- + P \tag{3}$$

$$(H_2PO_2)^{2-} + H_2O = H^+ + (HPO_3)^{2-} + H_2 \tag{4}$$

In Eq. (2), the adsorbed active hydrogen reduces the nickel at the surface of the catalyst. Hydrogen absorption reduces the hypophosphite at the catalytic surface to water, hydroxyl ion and phosphorus as shown in Eq. (3). Simultaneously, most of the hypophosphite was present in the catalyst, which was oxidized to orthophosphate and gaseous hydrogen as shown in Eq. (4).

In this mechanism, vapor and hydrogen gas formed by reaction blocked the entrance of the alumina nano-channels. In addition, the more the ENP temperature increased, the faster these gases formed. As the ENP temperature increased, the formation of gases became faster. In the ENP at 90 °C, nickel particles formed in the upper part of the nano-channels as shown in Figure 2(b). The entrances of the pore channels processed at 90 °C were blocked by the nickel formation in the early processing period. In the case of ENP at 60 °C, nickel particles were formed up to the bottom of the nano channels. Lower processing temperatures improved the nickel penetration depth during ENP. The total electrode area of spherical nickel particles that is contacted to alumina surface was larger than the other shape of nickel because of the cusp shape of alumina in the nano-channel, as shown in Figure 2(c). Alumina material and the deposited nickel particles were observed by EDS as shown in Figure 2(d).

Figure 3 shows the microstructure along the alumina nano-channels. An inner surface of the alumina was formed by hydration during the anodizing process as shown in Figure 3(a).

The spherical nickel particles formed by ENP were fully covered on the alumina inner surfaces as shown in Figure 3(b). A partially contacted interfaces between the alumina and the nickel particles were formed by hydrogen generation during the ENP process. These pores between nickel and alumina reduced the capacitance density of the alumina film capacitors.

Figures 3(c) and (d) show the cross section views treated by FIB of the middle of the alumina nano-channels with nickel electrodes. The nickel particles fully covered the alumina inner surfaces.

Figure 4 shows the electrical properties of the all solid capacitors made by ENP at various processing temperatures: leakage current (LC), break down voltage (BDV)

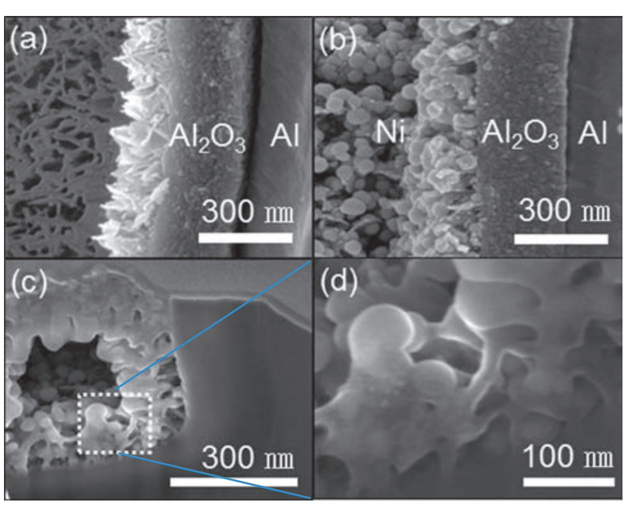

Figure 3. SEM images for inner part of (a) the alumina nano-channels without nickel particles, (b) alumina nano-channels with nickel particles made by ENP at 60 °C. Cross-section of alumina nano-channels with nickel electrode treated by FIB: (c) alumina nano-channels with spherical nickel layers coated by ENP at 60 °C, and (d) high magnification.

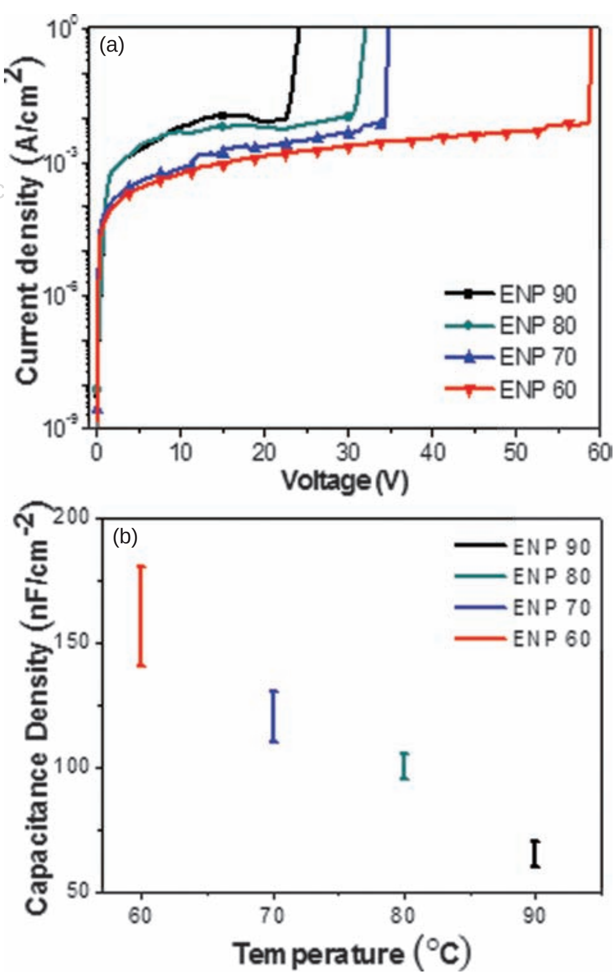

Figure 4. (a) Current–voltage characteristics and (b) capacitance densities of alumina film capacitors at various ENP processing temperatures.

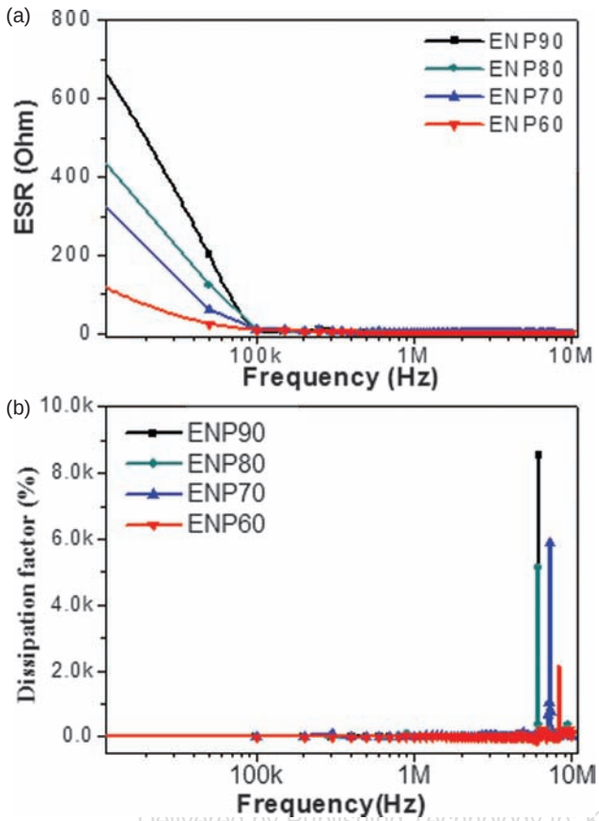

Figure 5. The variation in (a) ESR values in 100 Hz to 10 MHz and (b) dissipation factors of the alumina film capacitors with various ENP processing temperatures.

and capacitance density (CD). As the ENP processing temperatures decreased, the LC and the BDV improved as shown in Figure 4(a). This is attributed that the nickel particles formed at 60 °C are deeply penetrated through the alumina nano-channels. Dense nickel electrode structures reduce the LC and increase the BDV in the $Al/Al_2O_3/Ni$ structure capacitors.

The electrical capacitance (C) is expressed as

$$C = \varepsilon_O \varepsilon_R \frac{A}{l}$$

where ε_O is the vacuum permittivity, ε_R is the specific dielectric constant of the dielectric film, l is the film thickness and A is the effective surface area.

As the effective surface area of the nickel electrode on the alumina nano-channels increased, the capacitance of the $Al/Al_2O_3/Ni$ structure increased as shown in Figure 4. ENP at 60 °C (ENP60) shows a capacitance density of 160 nF/cm^2 due to the high effective surface due to the good nickel penetration through the alumina nano-channels. A dense nickel electrode showed the lowest LC.

As shown in Figure 5, ENP60 had a lower equivalent series resistance (ESR) values as a function of frequencies than the other results. It was found that the enhanced ESR properties of the thin film capacitor lowered the frequency dependence of capacitance in the frequency range of 100 kHz to 1 MHz and decreased the heat generation and electric power consumption.

In addition, ENP60 showed a high ESR value resulting from the contact resistance at the alumina and the nickel electrodes.

4. CONCLUSION

All solid capacitors were fabricated using alumina nano-channels with nickel electrodes by ENP at 60 °C, which showed a good capacitance density of 160 nF/cm^2 and superior performance in the high frequency range, as well as a lower LC, DF and ESR. Lower processing temperatures improved the nickel penetration depth during ENP. The total electrode area of spherical nickel particles that is contacted to alumina surface was larger than the other shape of nickel because of the cusp shape of alumina in the nano-channels.

Acknowledgments: The study was supported by the KIST (Korea Institute of Science and Technology) Future Resource Program (2E24871).

References and Notes

1. W. J. Sarjeant, J. Zirnheld, F. W. MacDougall, J. S. Bowers, N. Clark, I. W. Clelland, R. A. Price, M. Hudis, I. Kohlberg, G. McDuff, I. McNab, S. G. Parler, Jr, and J. Prymak, Handbook of Low and High Dielectric Constant Materials and Their Application, edited by H. S. Nalwa, Academic, UK **(1999)**, Vol. 2, pp. 424–490.
2. A. Nishino, *J. Power Sources* 60, 137 **(1996)**.
3. J. H. Jang, C. H. Lee, W. S. Choi, N. J. Kim, T. Y. Kim, T. Y. Kim, and S. J. Suh, *J. Vac. Sci. Technol. B* 28, 1231 **(2010)**.
4. J. H. Jang, T. Y. Kim, C. H. Lee, J. J. Zhang, E. M. Park, C. Park, and S. J. Suh, *Jpn. J. Appl. Phys.* 50, 071502 **(2011)**.
5. W. P. Dow, M. Y. Yen, W. B. Lin, and S. W. Ho, *J. Electrochem. Soc.* 152, C769 **(2005)**.
6. T. Kobayashi, J. Kawasaki, K. Mihara, and H. Honma, *Electrochim. Acta* 47, 85 **(2001)**.
7. C. S. Jun and K. H. Lee, *J. Membr. Sci.* 176, 121 **(2000)**.
8. C. H. Ting, M. Paunovic, P. L. Pai, and G. Chiu, *J. Electrochem. Soc.* 136, 2 **(1989)**.
9. Z. Wang, O. Yaegashi, H. Sakaue, T. Takahagi, and S. Shingubara, *J. Electrochem. Soc.* 151, C781 **(2004)**.
10. R. C. Agarwala and V. Agarwala, *Sadhana* 28, 475 **(2003)**.
11. D. W. Baudrand, Electroless Nickel Plating, Surface Engineering, ASM Hand Book, American Society for Materials, Material Park, Ohio **(1994)**, Vol. 5, pp. 290–298.
12. R. A. Khosroshahi and N. P. Ahmadi, *Asian J. App. Sci.* 2, 83 **(2009)**.

Received: 25 March 2014. Accepted: 18 June 2014.